Korean J. Chem. Eng., 35(11), 2256-2268 (2018)
DOI: 10.1007/s11814-018-0086-9

pISSN: 0256-1115
eISSN: 1975-7220

Sublayer assisted by hydrophilic and hydrophobic ZnO nanoparticles toward engineered osmosis process

Sina Mansouri*, Soodabeh Khalili, Majid Peyravi**, Mohsen Jahanshahi**,†, Rezvaneh Ramezani Darabi**, Fatemeh Ardeshiri***, and Ali Shokuhi Rad*****

*School of Chemical Engineering, Kavosh Institute of Higher Education, Mahmood Abad, Iran
**Membrane Research Group, Nanotechnology Institute, Babol Noshirvani University of Technology, Shariati Ave., Babol, 47148-71167, Iran
***Institute of Nanoscience and Nanotechnology, University of Kashan, Kashan, Iran
****Department of Chemical Engineering, Qaemshahr Branch, Islamic Azad University, Qaemshahr, Iran
(*Received 31 December 2017 • accepted 27 May 2018*)

Abstract−Hydrophilic and hydrophobic polyethersulfone (PES)-zinc oxide (ZnO) sublayers were prepared by loading of ZnO nanoparticles into PES matrix. Both porosity and hydrophilicity of the hydrophilic sublayer were increased upon addition of hydrophilic ZnO, while these were decreased for the hydrophobic sublayer. In addition, the results demonstrated that the hydrophilic membrane exhibited smaller structural parameter (*S* value or *S* parameter or *S*), which is beneficial for improving pure water permeability and decreasing mass transfer resistance. In contrast, a higher *S* parameter was obtained for the hydrophobic membrane. With a 2 M NaCl as DS and DI water as FS, the pure water flux of hydrophilic TFN0.5 membrane was increased from 21.02 L/m^2 h to 30.06 L/m^2 h and decreased for hydrophobic TFN0.5 membrane to 14.98 L/m^2 h, while the salt flux of hydrophilic membrane increased from 10.12 g/m^2 h to 17.31 g/m^2 h and decreased for hydrophobic TFN0.5 membrane to 3.12 g/m^2 h. The increment in pure water permeability can be ascribed to reduction in *S* parameter, which resulted in reduced internal concentration polarization (ICP). The current study provides a feasible and low cost procedure to decrease the ICP in FO processes.

Keywords: ZnO Nanoparticles, Hydrophilic and Hydrophobic Sublayer, Thin Film Composite Membrane, *S* Parameter, Forward Osmosis

INTRODUCTION

Forward osmosis (FO) as a promising membrane technology for desalination process is driven by osmotic pressure gradient across a permeable membrane [1-3]. The membrane is the nucleus of the FO process, and hence numerous researches have been carried out to tailor the FO membrane structure for efficiency optimization [4-6]. Cellulose triacetate (CTA) membranes fabricated are the most popular FO membranes for water purification and desalination processes. However, CTA FO membrane suffers from poor salt rejection and water permeability. Besides, the thin film composite (TFC) membranes have been newly considered as an alternative to dense asymmetric membranes, as they demonstrate higher salt rejection and water flux. The high production rate of pure water could be due to the thin active layer, which presents lower water transport resistance [7-11]. Nevertheless, despite such remarkable improvement in recent years in FO membrane optimization, more efforts are needed. The main barrier in practical FO applications contains the much-diminished efficient of osmotic pressure gradient caused by concentration polarization (CP), especially internal CP (ICP) in the membrane sublayer [12,13]. ICP is an inherent phenomenon of the osmosis driven system, because of the draw solution (DS) dilution around the sublayer and accumulation of the feed solution (FS) solutes around the active layer. This ICP phenomenon is different from the external CP, often faced with pressure driven processes as it happens inside the porous sublayer of the membrane. Hence, the dramatic waste in the effective driving force created by ICP cannot be omitted by increasing the turbulence and cross-flow velocity along the surface [14-16]. In FO processes, one of the most serious problems is to calculate the degree of ICP, since it cannot be calculated directly [17]. To investigate the ICP effects on the water flux of FO processes, a structural parameter (*S* value, *S* parameter or *S*) is frequently employed. A solution for decreasing ICP during FO processes is to decrease the value of the *S* parameter for the sublayer. By decreasing the *S* parameter of the sublayer, the mass transfer resistance decreases and following that the ICP is decreased [18]. Theoretically and physically, since the *S* parameter only consists of intrinsic characteristics of membranes such as sublayer tortuosity, porosity and thickness, it should be consistent irrespective of operating conditions – containing FS and DS concentrations – in which the same FO membrane is utilized. A smaller *S* parameter can be obtained by enhancing porosity, lowering tortuosity and thinning the sublayer structure. In addition to the ICP in osmotically driven processes, opposite diffusion of the salt from the DS through the membrane to the FS is also unavoidable because of the concentration differences [19-21]. Reverse salt diffusion is not favor-

†To whom correspondence should be addressed.
E-mail: mmohse@yahoo.com

able, as it will lead to increased ICP and the accumulation of DS in the FS that may raise the bulk FS concentration as well as induce fouling in the FO membrane [22-24]. The above discussion makes clear that reverse DS diffusion into the FS is a critical area that requires further study for FO application. For FO membrane fabrication, the structure of the membrane sublayer is critical, because it not only provides sublayer mechanical resistance and water flow pathways, but it also controls the degree of ICP phenomenon through the improvement of the osmotic driving force for water molecule movement across the final FO membranes [25,26]. The loading of inorganic nanoparticles as a sublayer developing strategy has shown to markedly improve the performance of the neat membranes in several aspects, such as thermal stability, permeability, mechanical strength and selectivity [5,27]. Zooming in specifically for FO membrane sublayer fabrication, Kuang et al. [20] incorporated calcium carbonate ($CaCO_3$) nanoparticles into PSf support layer, resulting in a notable decrease of *S* parameter from 4,834 μm to 796 μm and a higher pure water permeability under either FO (rejection layer facing FS) or PRO (rejection layer facing DS) orientation. The author ascribed this reduction to the increased porosity, decreased mass transfer resistance and bringing continuous channels for water and ion transportation. Ghanbari et al. [28] synthesized polysulfone-nano-composite sublayer membranes by incorporating halloysite nanotubes (HNTs) in polysulfone sublayers. The PSfN0.5 (with 0.5 wt% HNTs loading) sublayer demonstrated an increase in porosity and hydrophilicity and a decrease in *S* parameter. The TFN membrane prepared from such sublayer membrane exhibited significantly enhanced pure water permeability compared to the neat membrane. More recently, Tian et al. [29] successfully embedded silica (SiO_2) nanoparticles in polyetherimide (PEI) nanofibrous sublayer for making TFN polyamide membranes to mitigate undesired ICP phenomenon. Results demonstrate that the fabricated TFN-FO membrane with the 1.6% SiO_2 loading could achieve maximum sublayer porosity, smallest *S* parameter and highest pure water permeability. Compared with other nanoparticles, zinc oxide (ZnO) has gained more attention because of its non-toxic nature, relatively low cost, environmentally friendly and mechanical and chemical stability [30].

The main purpose of current work was to study the effect of hydrophilic and hydrophobic modified ZnO nanoparticles incorporated in the membrane sublayer on FO membrane properties. Further, we wanted to find how changes in the sublayer morphology could affect the ICP phenomenon, followed by *S* parameter as well as the water flux and reverse salt flux of the TFC/TFN membrane when examined in FO process. To the best of our knowledge, this is the first study comparing hydrophilic and hydrophobic sublayer on TFN membrane using PES-ZnO nanocomposite sublayer for FO applications.

EXPERIMENTAL

1. Materials

Dimethylformamide (DMF, >99.8%, Merck), polyethersulfone (PES, ultrason 6020) and polyvinyl pyrrolidone (PVP, Sigma) were used as solvent, polymer and additive for sublayer synthesis, respectively. Materials used for synthesis of active layer included m-phenylene diamine (MPD, >95%, Merck), n-hexane (>99%, Merck) and 1,3,5-benzenetricarbonyl trichloride (TMC, >98%, Merck). Sodium chloride (NaCl, >99.5%, Merck) was used to prepare the salt permeability test as well as FS and DS examination in FO operation. Materials used for the synthesis of hydrophilic and hydrophobic modified ZnO NPs included zinc nitrate hexahydrate ($Zn(NO_3)_2 \cdot 6H_2O$, Merck), n-Octyltriethoxysilane (n-OTES, Merck), ethanol (99.8%, Merck), acetone (99.8%, Merck) and sodium carbonate (Na_2CO_3, Merck).

2. Hydrophilic and Hydrophobic ZnO Nanoparticles

Hydrophilic ZnO nanoparticles were synthesized by a precipitation procedure similar to that described by Abbasian et al. [31]. Two initial solutions were prepared as follows: solution (1) 29.747 gr Zn $(NO_3)_2 \cdot 6H_2O$ dissolved in 1L DI water, and solution (2) 12.718 gr Na_2CO_3 dissolved in 1L DI water. Solution (1) was added to the solution (2) under stirring. The resulting mixed solution was filtered, centrifuged and washed with DI water three times. The solid powders were washed with ethanol and acetone and dried in an oven at 60 °C for 6 hr. Finally, ZnO hydrophilic nanoparticles were generated after calcination of white solid powders at 250 °C for 2 hr. To synthesize the hydrophobic ZnO nanoparticles, first 1 gr of hydrophilic ZnO nanoparticle and 2 ml APTES were dispersed in 50 ml ethanol; after that the resulting solution was stirred and refluxed at 70 °C for 24 hr. After centrifugation of the obtained product, hydrophobic ZnO nanoparticles were washed with ethanol and acetone and then dried in vacuum oven at 50 °C for 24 h [32].

3. Membrane Preparation

Membrane support layers were prepared to adapt the procedure from our previous work as described in Supporting Information (SI) [33]. Nine different FO sublayers were fabricated utilizing PES casting solutions as illustrated in Table 1. The rejection layer was synthesized on the PES support layer by IP process according to our previous work as described in SI [33].

4. Characterization

FTIR spectrometer (model: TENSOR 27, Germany) was employed to study the functional groups of hydrophilic and hydrophobic ZnO nanoparticles. The XRD patterns of the hydrophilic and hydrophobic ZnO nanoparticles were recorded at 2θ starting from 10° to 80° by X-ray diffractometer (JCPDS card no. 21-1272). Field emission scanning electron microscopy (FESEM, Model: Mira 3-XMU) was performed to determine the size and morphology of

Table 1. Preparation conditions of sublayer

Sublayer	PES (wt%)	PVP (wt%)	DMF (wt%)	Hydrophilic ZnO (wt%)	Hydrophobic ZnO (wt%)
PES	14	2	84.00	0	-
PES0.1	14	2	83.90	0.1	-
PES0.2	14	2	83.80	0.2	-
PES0.5	14	2	83.50	0.5	-
PES1	14	2	83.00	1	-
PES'0.1	14	2	83.90	-	0.1
PES'0.2	14	2	83.82	-	0.2
PES'0.5	14	2	83.50	-	0.5
PES'1	14	2	83.00	-	1

the hydrophilic and hydrophobic ZnO nanoparticles. Also, the morphology of the sublayer and TFC and TFN composite membranes was observed by FESEM images. To evaluate membrane hydrophilicity, water contact angle was performed by a contact angle goniometer (KRUSS BmbH, Germany). Before testing, the membrane samples were dried at ambient temperature for 24 h. Five measurements for each sample were evaluated to decrease experimental error. Because of the capillary effect, the measurements of water contact angle alone cannot enough predict the membrane hydrophilicity. Hence, to estimate the hydrophilicity accurately, solid-liquid interfacial energy ($-\Delta G_{SL}$) was calculated. High values of interfacial free energy mean higher surface hydrophilicity as a result of higher surface interaction between the liquid water droplet and solid sublayer. The $-\Delta G_{SL}$ can be calculated using contact angle as follows:

$$-\Delta G_{SL} = \gamma_L\left[1+\frac{\cos\theta}{\Delta}\right]$$

where θ, γ_L, and Δ are the contact angle value, the liquid surface tension (γ_L=72.8 m_J/m_2 for water at ambient temperature), and the relative surface area, respectively [34].

Sublayer porosity ε (%) was evaluated by measuring the wet mass (m_w, g) and dry mass (m_d, g) of sublayer according to the following [35]:

$$\varepsilon = \frac{(m_{wet}-m_{dry})/\rho_w}{((m_{wet}-m_{dry})/\rho_w)+(m_{dry}/\rho_m)}\times 100$$

where ρ_w (g/cm^3) indicates water density and ρ_m (g/cm^3) indicates sublayer density.

Guerout-Elford-Ferry equation (Eq. (9)) was used to determine sublayer mean pore size (r_m, μm) based on the flux and porosity data [36].

$$r_m = \sqrt{\frac{(2.9-1.75\varepsilon)\times(8\eta l Q)}{\varepsilon\times A\times\Delta P}}$$

Here, η indicates the water viscosity (8.9×10^{-4} Pa s), l (m) refers to the sublayer thickness and Q (m^3/s) is the volume of permeate per unit time.

RESULTS AND DISCUSSION

1. ZnO Nanoparticles Characterization

Fig. 1 demonstrates the FTIR spectra of hydrophilic and hydrophobic modified ZnO nanoparticles. The wide peak between 3,400 cm^{-1} and 3,450 cm^{-1} corresponds to the -OH groups of ZnO nanoparticles. Four extra peaks demonstrated by hydrophobic modified ZnO nanoparticles at 2,920 cm^{-1}, 2,870 cm^{-1}, 1,050 cm^{-1} and 890 cm^{-1} correspond to the CH_3, CH_2, Si-o and Zn-o-Si, respectively, which confirmed the successful modification of ZnO nanoparticles with n-OTES [37]. The size and structure of the ZnO nanoparticles were investigated by FESEM images. As shown in Fig. 2, the average size of the prepared ZnO nanoparticles is less than 30 nm with the morphology of quasi-spherical shapes. Further, the uniform size distribution ZnO nanoparticles can be important where they tend to disperse within the scaffold of PES sublayer well. Fig. 3 shows the crystal structures of ZnO nanoparticles investigated

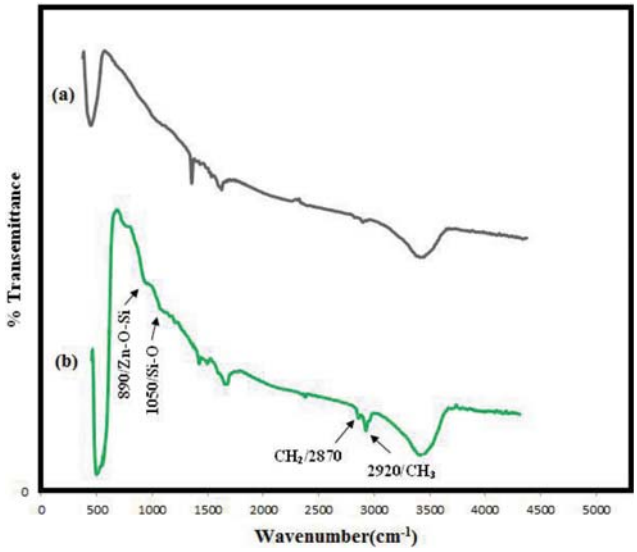

Fig. 1. FTIR spectra of (a) hydrophilic nanoparticles and (b) hydrophobic modified ZnO nanoparticles.

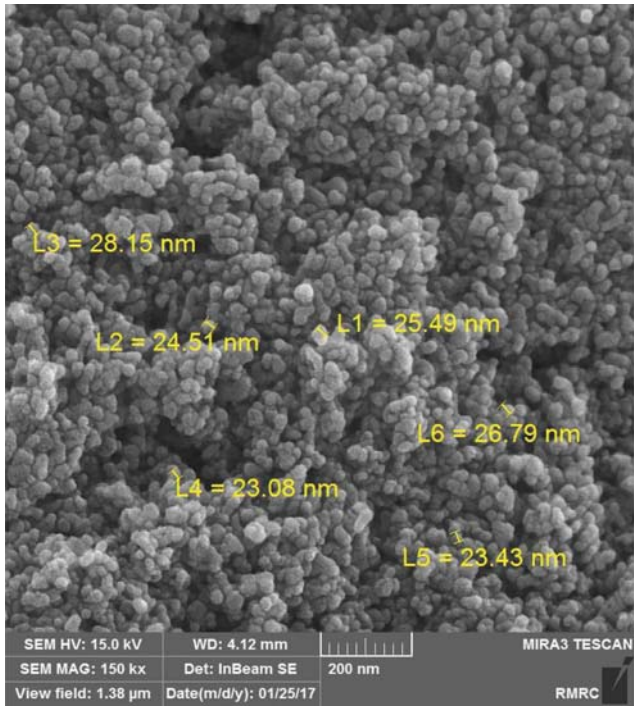

Fig. 2. The FESEM image of ZnO nanoparticle.

by XRD patterns. There are eleven major diffraction peaks at 31.8°; 34.45°; 36.2°; 47.6°; 56.6°; 62.89°; 66.4°; 67.9°; 69.1°; 72.6° and 74.91° observed for the ZnO nanoparticles [38]. To specify the hydrophilic and hydrophobic nature of ZnO nanoparticles, a dispersion experiment was performed by n-hexane (as non-polar solvent) and deionized water (as polar solvent). Each of the nanoparticles demonstrated significant distinct behavior in water and n-hexane. As shown in Fig. 4, the hydrophilic ZnO nanoparticle precipitated in the n-hexane, while easily dispersed in the deionized water because of its hydroxyl group. On the other hand, hydrophobic ZnO

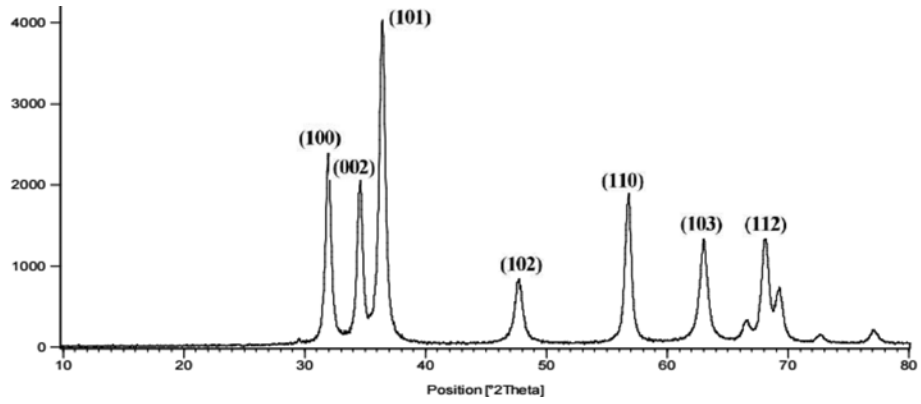

Fig. 3. XRD patterns of ZnO nanoparticle.

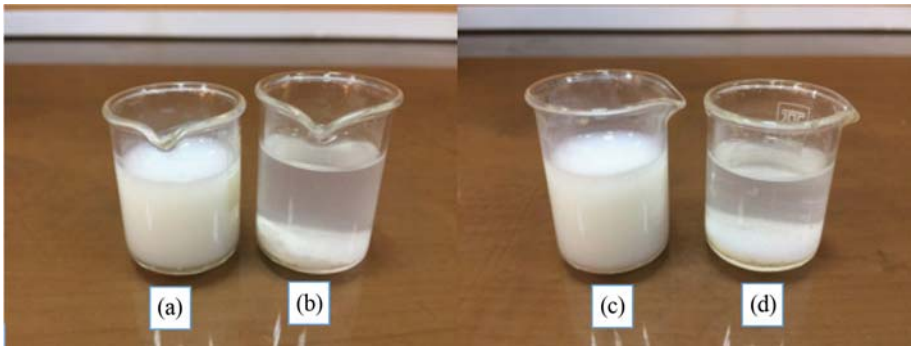

Fig. 4. Dispersion of the hydrophilic and hydrophobic nanoparticles in water and n-hexane, (a) hydrophilic nanoparticles in water, (b) hydrophilic nanoparticles in n-hexane (c) hydrophobic nanoparticles in n-hexane and (d) hydrophobic nanoparticles in water.

Table 2. Effects of the hydrophilic and hydrophobic ZnO loading on the properties of sublayer with respect to contact angle, thickness, overall porosity and pore size

Membrane	Contact angle (°)	Overall porosity (%)	Thickness (μm)	Mean pore sizes (nm)	Surface interfacial energy
PES	56.04±0.83	80.0±0.3	118.05±1.61	25.54±0.81	113.00
PES0.2	45.97±0.96	82.4±0.5	112.72±1.35	28.1±0.95	-
PES0.5	31.57±0.69	84.2±0.4	93.53±1.23	27.0±0.77	134.61
PES'0.2	65.27±1.11	79.3±0.3	113.71±1.46	22.1±0.61	-
PES'0.5	71.13±1.35	78.4±0.2	97.23±1.29	18.9±0.58	96.01

nanoparticle suspended in the n-hexane, while precipitated in deionized water. This features can be attributed to the silane groups. This distinct behavior of hydrophobic ZnO in n-hexane and water can be attributed to high affinity of hydrophobic ZnO nanoparticles (silane groups) into n-hexane that resulted in hydrophobic nanoparticles well dispersed in nonpolar solvent [39].

2. Induced PES Sublayer by Hydrophilic and Hydrophobic ZnO Nanoparticles

Table 2 demonstrates the changes in the PES support layer properties upon addition of hydrophobic and hydrophilic ZnO nanoparticles, and Table 3 demonstrates the water permeability and *S* parameter of the sublayer. As expected, the water permeability of the hydrophilic PES sublayer was increased from 148.89 L/m^2 h to 263.42 L/m^2 h, while the water permeability of the hydrophobic PES sublayer decreased from 148.89 L/m^2 h to 80.44 L/m^2 h. A reason-

Table 3. Effects of the hydrophilic and hydrophobic ZnO loading on the properties of sublayer with respect to pure water permeability and *S* value

Membrane	Pure water permeability (L/m^2 h bar)	*S* value (mm)
PES	148.89±7.23	0.58±0.04
PES0.1	180.20±8.58	0.52±0.03
PES0.2	201.08±8.74	0.48±0.03
PES0.5	232.90±9.28	0.40±0.04
PES1	263.42±9.14	0.34±0.02
PES'0.1	128.73±7.12	0.68±0.05
PES'0.2	114.09±7.34	0.72±0.05
PES'0.5	95.62±6.54	0.83±0.06
PES'1	80.44±7.69	1.02±0.09

able explanation for the improvement in water permeability of hydrophilic PES sublayer is the enhancement in interfacial energy coupled with the changes in sublayer properties. The interfacial energy calculated using the relative surface area and the contact angle gives the surface hydrophilicity quantitative analysis. The higher values of interfacial energy suggest higher surface hydrophilicity and vice versa [34]. As can be seen in Table 2, the PES membrane had a pure water contact angle of 56.04° and interfacial energy of 113.00 mJ/m^2. However, by addition of hydrophilic ZnO nanoparticles, the pure water contact angle decreased to 45.97° and then to 31.57° for PES0.5. As a consequence, the interfacial energy also enhanced from 113.00 mJ/m^2 to 134.61 mJ/m^2, demonstrating that the addition of hydrophilic ZnO nanoparticles enhanced the surface hydrophilicity of the PES membranes. The surface hydroxyl

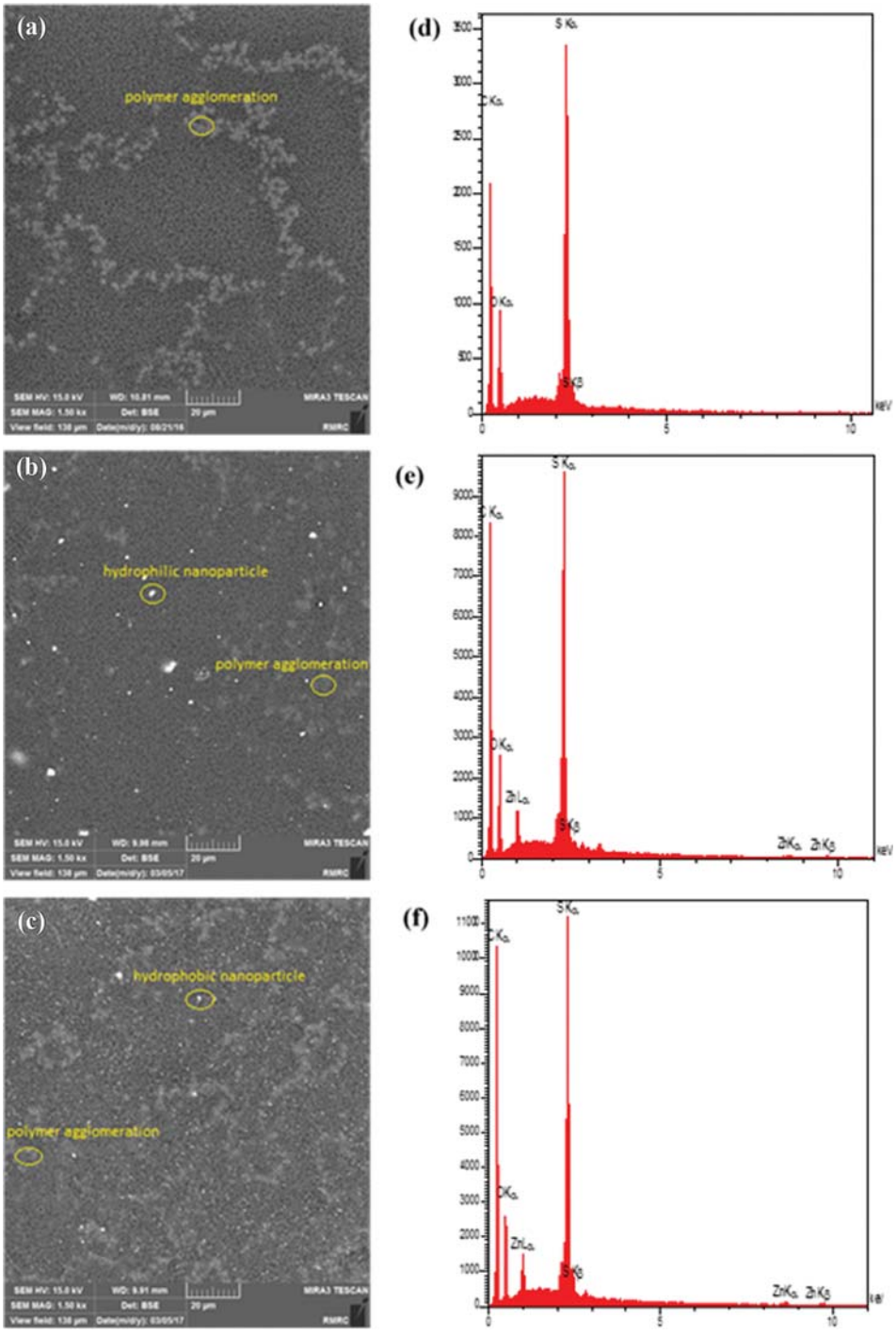

Fig. 5. Surface FESEM images of membrane sublayer using a backscattered imaging detector and EDX patterns for membrane sublayer, (a) FESEM images of PES membrane, (b) FESEM images of PES0.5 membrane, (c) FESEM images of PES'0.5 membrane, (d) EDX patterns for PES membrane, (e) EDX patterns for PES0.5 membrane and (f) EDX patterns for PES'0.5 membrane.

groups and the hydrophilic nature of the ZnO nanoparticles play an essential role in increasing the hydrophilicity of the hydrophilic PES membranes. For hydrophobic modified ZnO membrane, the contact angle increased to 71.13° and interfacial energy decreased to 96.01°. These two factors demonstrated that the addition of hydrophobic ZnO nanoparticles decreased the PES membranes surface hydrophilicity. Improving the hydrophilicity of the sublayer surface increases the tendency of water molecules to PES polymers and, consequently, enhances water permeability owing to the foundation of hydrogen bonds with water molecules. This hydrogen bonding between sublayer and water molecules causes a destructuring of the water complexes and facilitates water molecules transport through the PES membrane [40-42]. The reduction in water permeability of hydrophobic PES sublayer can be explained by increased membrane hydrophobicity and decreased overall porosity and pore sizes. Sublayer hydrophobicity was hence considered as a possible barrier to water flux across the PES membrane. If the membrane sublayer does not wet when exposed to the DI water, then water molecules transport is hindered through the sublayer [43]. Moreover, the pore size and porosity of the PES sublayer increased by hydrophilic ZnO nanoparticles loading and decreased by hydrophobic ZnO nanoparticles loading. As can be seen in Table 2, for the hydrophilic membrane, the increases of the pore size and porosity are mainly ascribed to the higher exchange rate of solvent (DMF) and non-solvent (DI water) because of the ZnO nanoparticles' affinity to water. Furthermore, for the hydrophobic membrane, the decreases of the pore size and porosity are mainly ascribed to the lower exchange rate of DMF and DI water because of hydrophobic nature of ZnO nanoparticles [28,44]. As observed in Table 3, the *S* parameter of the sublayer with hydrophilic nanoparticles was decreased by increasing nanoparticles loading and the *S* parameter of sublayer with hydrophobic nanoparticles was increased by

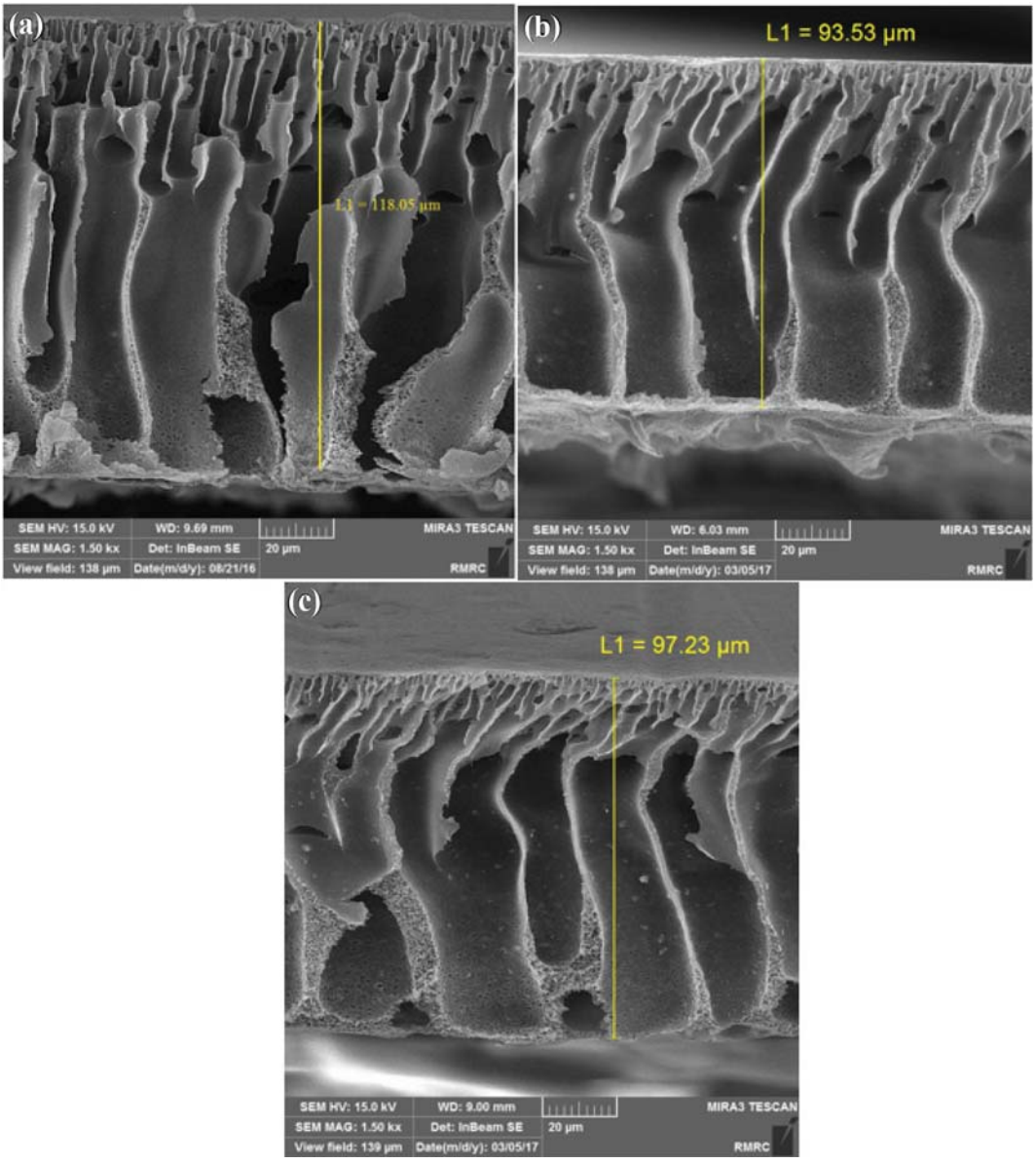

Fig. 6. Cross section FESEM morphologies of membranes sublayer, (a) PES, (b) PES0.5 and (c) PES'0.5.

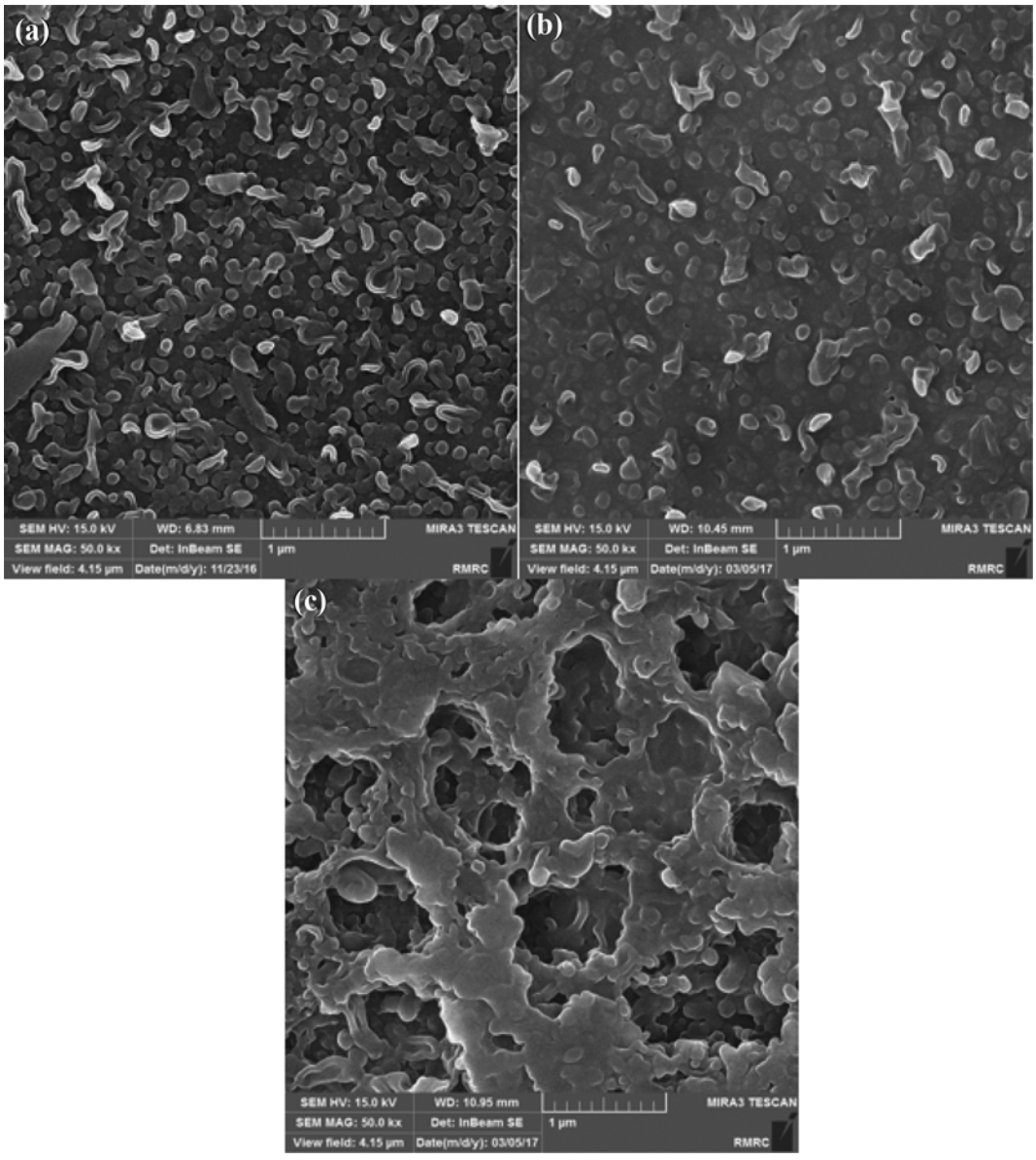

Fig. 7. FESEM images of FO membranes, (a) top surface of control membrane, (b) top surface of TFN0.5 membrane, (b) top surface of TFN'0.5 membrane.

adding nanoparticles. An increase in the porosity of the hydrophilic sublayer leads to a remarkable reduction in mass transfer resistance and operates as the major contributor for smaller *S* parameter. Overall, a smaller *S* parameter means a better sublayer, which can minimize ICP during FO process; hence higher pure water permeability will be obtained [19]. Fig. 5 demonstrates the existence of ZnO nanoparticles on the surface of the PES sublayer. The permanent attachment of these nanoparticles to the PES sublayer is due to the combination effects of chemical and physical interactions. By comparing PES0.5 and PES'0.5, the white spots which demonstrate nanoparticles and were confirmed by EDX analysis, in PES'0.5 are observed abundantly and distributed more uniformly than PES0.5 at the identical loading of ZnO nanoparticles. Also, the larger observed white spots in backscattered SEM image of PES0.5 show that agglomeration was done between hydrophilic ZnO nanoparticles because of the hydrophilic-hydrophilic interactions between nanoparticles when they were dispersed in hydrophobic media of PES casting solution. In contrast, the hydrophobically modified ZnO nanoparticles can be easily distributed within the hydrophobic PES chains due to the hydrophobic compatibility of ZnO nanoparticles and PES chains. Fig. 6 illustrates the images of cross section of three PES sublayers used for TFC and TFN membrane preparation. The overall thickness of PES0.5 and PES'0.5 was lower than neat PES. In fact, the reduced thickness resulting from ZnO loading is one of the factors contributing to smaller *S* parameter [45].

3. Membranes Prepared from Hydrophilic and Hydrophobic Sublayer

The top surface and cross-section morphology of three FO membranes were analyzed using FESEM techniques, and the results are illustrated in Figs. 7 and 8. In the top surface images, the white parts

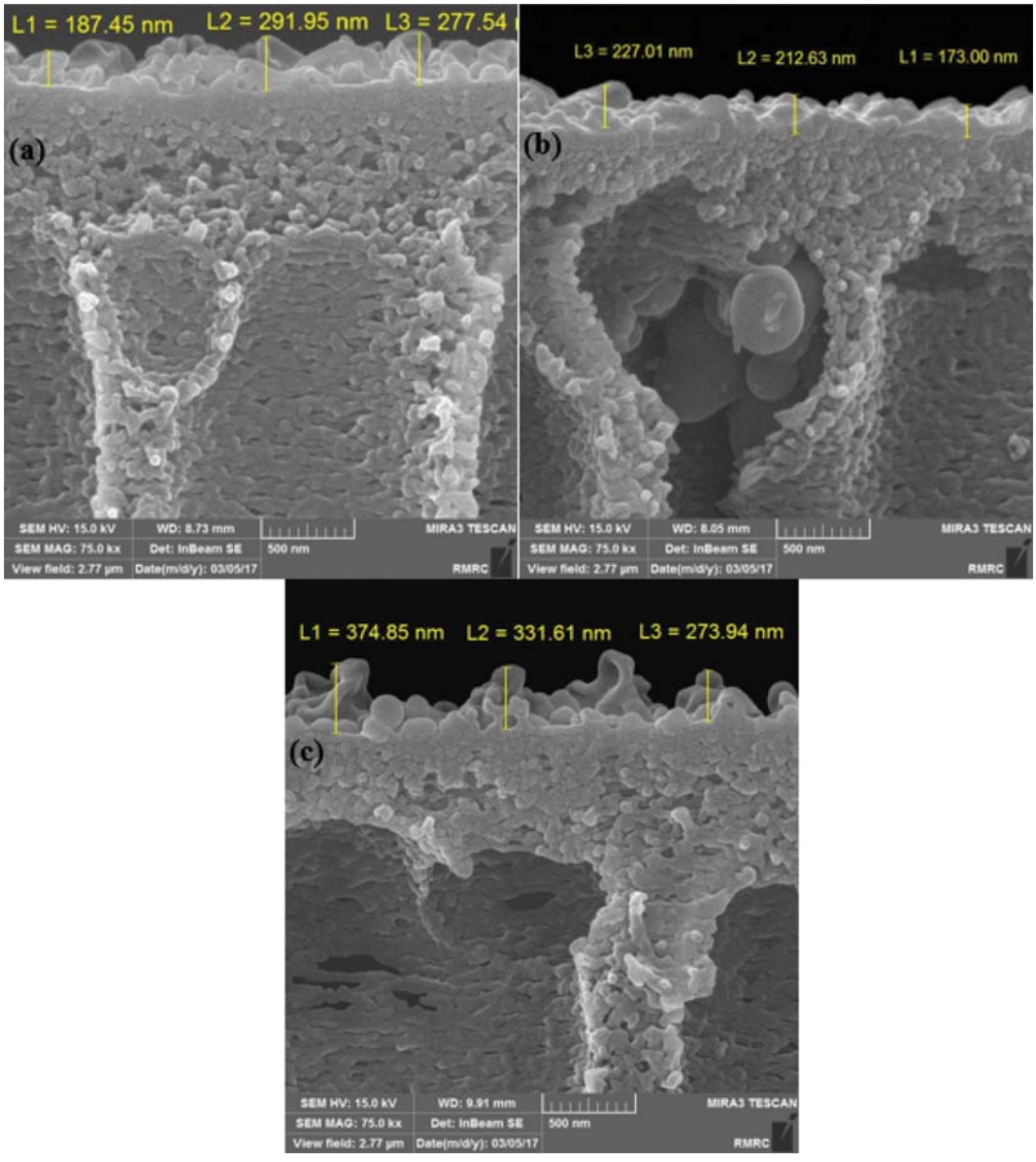

Fig. 8. FESEM images of FO membranes, (a) cross section of control membrane, (b) cross section of TFN0.5 membrane, (b) cross section of TFN'0.5 membrane.

demonstrate the peaks, while the dark areas represent the valleys. The change in the top surface morphology of TFC and TFN membranes compared to the PES sublayer confirms that PA layer was successfully formed over PES sublayer. Clearly, there was a variation in PA active layer structure by employing different sublayers. All membranes represented uniformly formed "ridge-and-valley" like structure. Moreover, the top surface of hydrophilic TFN membrane includes numerous nodular structures [46]. In comparison to the TFC membrane, the hydrophilic TFN membranes have a more open top surface morphology. This type of morphology can be beneficial to facilitating water passing, resulting in improved pure water permeability. For hydrophobic membrane, the sublayer tended to cover the valley portion and increased the ridge portion of active layer. This, as a conclusion, resulted in the increment in active layer thickness as demonstrated in the cross-sectional image of the hydrophobic TFN membrane. The difference in density of the polyamide layer prepared over the different sublayers is remarkable evidence that the formed top layers were altered by the sublayer characterization. Since the interfacial polymerization parameters remain unchanged during the construction of the TFC membrane, the differences of active layer thickness as well as the surface morphology provide remarkable evidence that the physical and chemical properties of sublayer greatly influence on the interfacial polymerization reaction. It is generally well recognized that the fabrication of active layer involves the reaction between MPD in the DI water aqueous solution soaked in the sublayer membrane with organic solution of TMC that covers the surface of the sublayer membrane. In principal, the interfacial polymerization reaction occurs in the organic solution at the interface between the aqueous phase and the organic phase [25,47]. Based on this argument, the diffusion of

MPD monomer through the DI water aqueous solution from the sublayer voids to the surface plays as a significant role in interfacial polymerization rate. The faster the MPD supply, the more is the opportunity of cross-linking constitution and, conversely, the slower the MPD supply there is more opportunity of linear polymer constitution [25]. As can be seen in Fig. 8, the membrane thickness for hydrophilic membrane was lower than that of hydrophobic membrane. For hydrophilic membrane, the hydrophilic groups in the sublayer surface may have an impression on the active layer formation. On one hand, these functional groups improve the sublayer hydrophilicity, which may be useful for wetting or soaking of sublayer with aqueous solution, and decreasing the defect formation chance. On the other hand, the functional groups of the hydrophilic sublayer may prevent the diffusion of amine during the interfacial polymerization. In this study, the surface hydrophilicity of hydrophilic PES sublayer was improved due to the OH group of hydrophilic ZnO nanoparticles, which contributed to the soaking of sublayer with aqueous solution. From this point of view, the diffusion rate of amine monomer from the pore structure to the hydrophilic membrane interface is affected by the presence of hydrophilic ZnO nanoparticles, and some of the amine monomers inside the voids may interact with ZnO through hydrogen bonding between hydrophilic ZnO nanoparticles and amine monomers. It has been formerly suggested that amine monomers diffuses slowly to the organic phase when hydrophilic functional groups of nanoparticles are present in the voids of the sublayer, resulting in a thinner active layer. For hydrophobic membrane, with an increasing sublayer hydrophobicity by adding hydrophobic ZnO nanoparticles, MPD is expected to diffuse more quickly due to no interaction between the MPD and the sublayer and resulting in a thicker active layer [47].

4. Performance in RO Mode

The different loadings effect of hydrophilic and hydrophobic ZnO nanoparticles on the flux and rejection of the modified membranes is demonstrated in Figs. 9 and 10. At operating pressure of 250 kpa, the control membrane tested with 40 mM NaCl solution demonstrated 4.71 L/m^2 h water flux and 92.12% NaCl rejection, while the hydrophilic TFN0.5 membrane exhibited water flux of 6.66 L/m^2 h and 89.99% NaCl rejection. On the other hand, hydrophobic TFN0.5 membrane exhibited water flux of 3.49 L/m^2 h and 96.56% NaCl rejection. It was suggested that incorporating hydrophilic ZnO nanoparticles can improve the water flux while

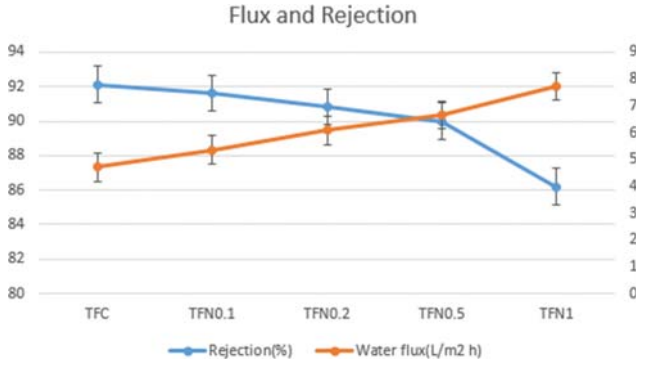

Fig. 9. Water flux and NaCl salt rejection of hydrophilic membranes.

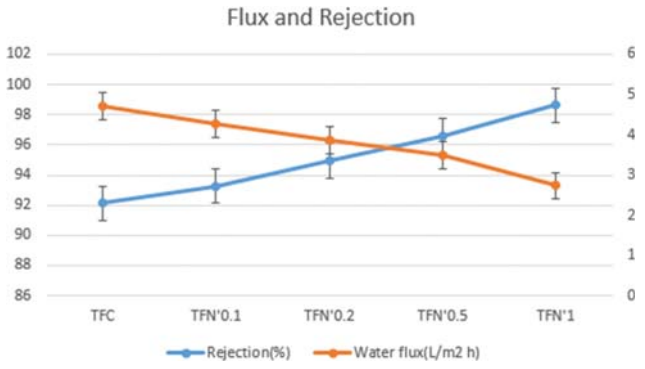

Fig. 10. Water flux and NaCl salt rejection of hydrophobic membranes.

the combination of hydrophobic ZnO nanoparticles with sublayer can improve the salt rejection. The improved water permeability of hydrophilic TFN membrane can be justified by three factors: (i) an increase of the sublayer porosity and hydrophilicity increases the pure water permeability, (ii) a decrease of the top layer thickness also increases pure water permeability, and (iii) an open type surface morphology of hydrophilic TFN membrane can be beneficial to facilitating water passage and increasing pure water permeability [48,49]. It seems that the formation of open type morphology and thinner polyamide layer are the major reasons for the decrease of NaCl rejection. A significant decrease in NaCl rejection is observed from TFN0.5 to TFN1, which is due to hydrophilic ZnO aggregation at high concentration. Also, the decreased water permeability of hydrophobic TFN membrane can be explained by three factors: (i) a decrease of the sublayer porosity and an increase of sublayer hydrophobicity decreases the water permeability, (ii) an increase of the top layer thickness also decreases water permeability, and (iii) eventually more crosslinking also decreases water permeability. Therefore, higher degree of crosslinking and thicker polyamide layer are the major reasons for the increase of rejection. Thus, in comparison to hydrophobic membrane with low water permeability and high salt rejection, the hydrophilic membrane with the pure water permeability and slightly lower salt rejection compared to TFC membrane is beneficial for FO application. Regarding to this point, comparisons with other studies were performed with hydrophilic membranes in our study and presented in Table 4 [50]. With respect to pure water permeability, the PES sublayer induced by ZnO played a main role in the enhancement membrane efficiency. All membranes prepared by PES-ZnO nanocomposite sublayer represented much higher pure water permeability than two of commercial membranes. With respect to NaCl permeability/pure water permeability (B/A) ratio, whole membranes produced in this study demonstrated smaller B/A values compared to the commercial membranes. The smaller B/A value demonstrates the better efficiency of our in-house TFC and TFN membranes in decreasing NaCl reverse diffusion during FO process [51].

5. Performance in FO Mode

A cross-flow process at FO mode was used to assess the pure water flux and salt flux of TFC and TFN membranes, and results are demonstrated in Table 5 and Figs. 11 until 14. 10 mM NaCl salt

Table 4. The separation properties of hydrophilic and hydrophobic membranes synthesized in this work

Membrane	Water permeability (L/m^2 h bar)	Water permeability A ($\times10^{-12}$ m/s Pa)	Salt permeability B ($\times10^{-8}$ m/s)	B/A (kPa)	References
TFC	1.88±0.19	5.22±0.29	11.16±1.61	21.38±3.23	In this work
TFN0.1	2.14±0.21	5.94±0.35	13.58±1.64	22.86±3.24	In this work
TFN0.2	2.43±0.24	6.75±0.43	17.05±1.86	25.26±3.35	In this work
TFN0.5	2.66±0.25	7.39±0.49	20.55±1.95	27.80±3.38	In this work
TFN1	3.09±0.28	8.58±0.58	34.31±2.23	39.99±4.28	In this work
TFN'0.1	1.70±0.18	4.72±0.28	8.51±1.55	18.02±3.01	In this work
TFN'0.2	1.54±0.18	4.28±0.28	5.69±1.43	13.29±2.44	In this work
TFN'0.5	1.40±0.17	3.89±0.26	3.46±1.29	8.89±1.26	In this work
TFN1	1.09±0.15	3.03±0.25	1.06±1.28	3.50±0.54	In this work
CTA-HW	1.19±0.19	3.3±0.50	25.60±1.4	84.00±8	[50]
CTA-W	0.33±0.04	0.9±0.10	4.00±0.9	47.00±12	[50]

Table 5. Comparison of FO membrane performance

Membrane	Water flux (L/m^2 h)	Reverse salt flux (g/m^2 h)	Feed solution	Draw solution	References
TFC	21.02±0.71	10.12±0.48	10 mM NaCl	2 M NaCl	In this work
TFN0.1	23.45±0.79	12.20±0.51	10 mM NaCl	2 M NaCl	In this work
TFN0.2	26.03±0.82	15.03±0.56	10 mM NaCl	2 M NaCl	In this work
TFN0.5	30.06±0.85	17.31±0.57	10 mM NaCl	2 M NaCl	In this work
TFN1	35.51±0.96	31.89±0.71	10 mM NaCl	2 M NaCl	In this work
TFN'0.1	18.21±0.65	8.01±0.42	10 mM NaCl	2 M NaCl	In this work
TFN'0.2	16.99±0.61	5.90±0.32	10 mM NaCl	2 M NaCl	In this work
TFN'0.5	14.98±0.57	3.12±0.18	10 mM NaCl	2 M NaCl	In this work
TFN'1	12.11±0.44	1.02±0.09	10 mM NaCl	2 M NaCl	In this work
TFC 21	17.0±0.9	43.00	DI water	2 M NaCl	[20]
TFC 3	24.2±1.2	19.00	DI water	2 M NaCl	[55]
CTA-HW	18.30	-	10 mM NaCl	2 M NaCl	[50]
CTA-W	12.10	-	1 mM NaCl	2 M NaCl	[50]

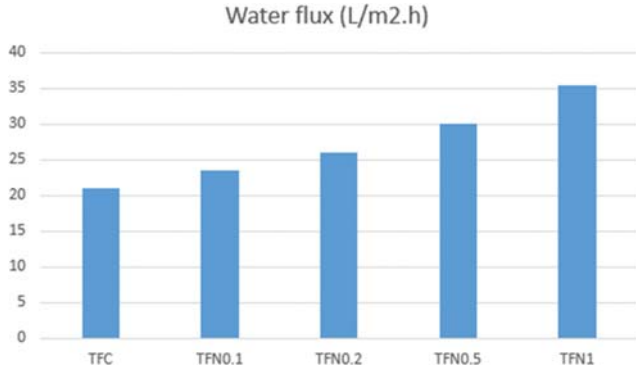

Fig. 11. Water flux of FO membranes prepared from hydrophilic PES sublayer.

was used as FS and 2 M NaCl salt was used as DS. Compared to the neat TFC membrane, the hydrophilic TFN membranes fabricated using PES-ZnO nanocomposite sublayer demonstrated higher water flux and reasonable salt flux while hydrophobic TFN membranes demonstrated lower salt flux and lower water flux. The higher pure water flux of the hydrophilic TFN membrane could be attributed to the increment in surface hydrophilicity and porosity of these hydrophilic membranes. This better structural property of hydrophilic PES-ZnO sublayer decreases the transportation resistance against water molecules permeation [52]. Furthermore, the lower pure water flux of the hydrophobic TFN membranes could be attributed to the reduction in porosity, pore size and surface hydrophilicity, and also attributed to intensifying water transport resistance due to the hydrophobic nature of ZnO nanoparticles. As can be observed in Fig. 11 and 12, with 0.5 wt% ZnO added, the pure water flux of hydrophilic TFN membrane was improved from 21.02 L/m^2 h of TFC to 30.06 L/m^2 h of hydrophilic TFN0.5 and decreased for hydrophobic TFN membrane to 14.98 L/m^2 h. The results suggest that adding hydrophilic ZnO nanoparticles into the PES sublayer of TFC membrane was an impressive way for enhancing FO membrane pure water flux by reducing the ICP phenomenon effect following a reduction in *S* parameter. Unlike RO membrane, which water molecule transport is often affected by the hydraulic insistence constructed by the TFC membrane structure,

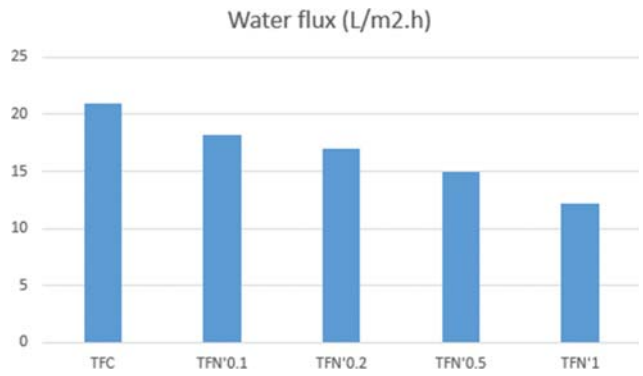

Fig. 12. Water flux of FO membranes prepared from hydrophobic PES sublayer.

in FO process, ICP in the sublayer of TFC membrane also substantially affects water molecule transport [53]. We believe that in lieu of modifying top layer properties, improving the PES sublayer properties by embedding hydrophilic ZnO nanoparticles could also be an impressive approach to enhance FO process performance by decreasing the effect of ICP phenomenon [52]. The salt fluxes of TFC and TFN membranes tested at FO orientation are demonstrated in Figs. 13 and 14. The trend of NaCl salt flux was correlated to the trend of salt rejection data in RO process, demonstrated in Figs. 9 and 10, where a high salt rejection corresponded to a low salt flux and vice versa. Note that there was an insignificant increment in salt flux by increasing ZnO concentration up to 0.5 wt% in comparison to TFC membrane. However, further increasing in loading of hydrophilic ZnO nanoparticles to 1 wt% was maybe to cause a lower degree of PA crosslinking, decreasing membrane performance in NaCl rejection and increasing its salt flux. As can be seen in Fig. 14, the salt flux of the hydrophobic TFN membranes was decreased from 10.12 g/m^2 h to 1.02 g/m^2 h. So, the hydrophobic membrane has low salt flux because of its high salt rejection. Furthermore, more hydrophobic surfaces demonstrate that these membranes would indicate less affinity to hydrophilic compounds and construct an interface, which is poor in polar solutes. Hence, these TFN membranes would have higher rejection against polar components compared to TFC membrane, which has lower water contact angles reported previously [54]. Based on the outcomes from the RO and FO experimental tests, it was deduced that 0.5 wt% hydrophilic ZnO nanoparticles was an optimum loading for PES-ZnO sublayer preparation to create promising efficiency of FO membrane with high pure water flux and low salt flux. Table 5 compares the pure water flux and salt flux of the membranes produced in the current study with others and commercial membrane [20,50,55]. Particularly, all the hydrophilic membranes synthesized in the current work have higher pure water flux and lower salt flux compared to others' work. This shows that FO membranes synthesized on sublayer with higher porosity and hydrophilicity can suffer a less intense ICP effect and achieve higher pure water permeabilities and lower reverse salt flux.

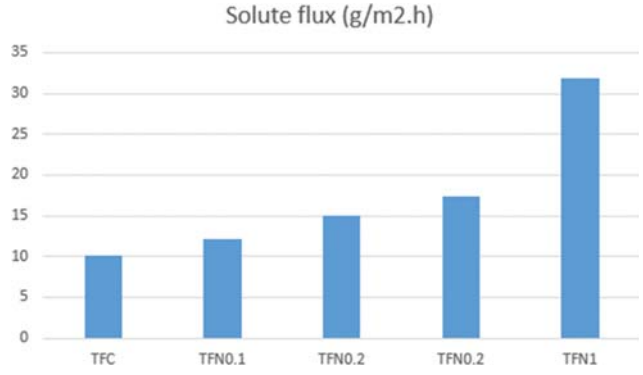

Fig. 13. Solute flux of FO membranes prepared from hydrophilic PES sublayer.

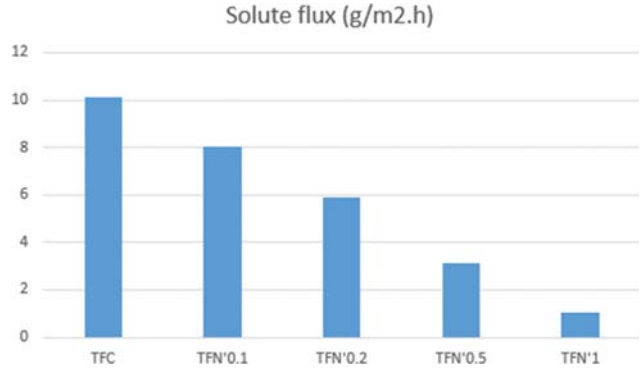

Fig. 14. Solute flux of FO membranes prepared from hydrophobic PES sublayer.

CONCLUSION

Hydrophilic and hydrophobic ZnO nanoparticles were synthesized and incorporated into PES sublayer for the preparation of the hydrophilic and hydrophobic FO membranes. For hydrophilic membranes, the hydrophilicity and porosity of the nanocomposite sublayer were improved, while for the hydrophobic membranes, the hydrophilicity and porosity of the sublayer were decreased. Moreover, an increment in hydrophilic ZnO nanoparticle loading at lower concentration increased pure water flux of hydrophilic TFN membranes during RO experimental test. The NaCl salt rejection of membranes until TFN0.5 membrane decreased from 92.12% to 89.99% upon addition of hydrophilic ZnO nanoparticles into PES matrix, but this reduction is very low and can be neglected against to increase in water flux. By further increasing ZnO nanoparticles loading to 1.0 wt%, the RO separation efficiency was significantly decreased and salt rejection reached 86.21%. For hydrophobic membranes, the water flux decreased and salt rejection increased in the RO test. According to the experimental outcomes, the hydrophilic TFN0.5 membrane represented the most satisfactory performance in FO process. Analysis of the sublayer *S* parameter suggested that addition of hydrophilic ZnO is an impressive strategy for reducing ICP phenomenon in FO processes, as the *S* parameter of hydrophilic TFN0.5 membrane was smaller in comparison to that of TFC FO membrane. Higher hydrophilicity and porosity and additional water pathways are the major factors for reducing in *S* value.

NOMENCLATURE

PES : polyethersulfone
ZnO : zinc oxide
CP : concentration polarization
ICP : internal concentration polarization
FO : forward osmosis
CTA : cellulose triacetate
TFC : thin film composite
TFN : thin film nanocomposite
DS : draw solution
FS : feed solution
$CaCO_3$: calcium carbonate
HNTs : halloysite nanotubes
SiO_2 : silica
PEI : polyetherimide
DMF : dimethylformamide
PVP : polyvinyl pyrrolidone
$-\Delta G_{SL}$: solid-liquid interfacial energy
MPD : M-phenylene diamine
TMC : 1,3,5-benzenetricarbonyl trichloride
NaCl : sodium chloride
(n-OTES) : N-Octyltriethoxysilane
$Zn(NO_3)_2 \cdot 6H_2O$: zinc nitrate hexahydrate
Na_2CO_3 : sodium carbonate
IP : interfacial polymerization
FESEM : field emission scanning electron microscopy
γ_L : liquid surface tension
ε : porosity
m_w : wet mass
m_d : dry mass
r_m : pore size
J : pure water flux
A : pure water permeability
B : salt permeability
J_s : reverse salt flux

SUPPORTING INFORMATION

Additional information as noted in the text. This information is available via the Internet at http://www.springer.com/chemistry/journal/11814.

REFERENCES

1. J. Heikkinen, H. Kyllönen, E. Järvelä, A. Grönroos and Ch. Y. Tang, *J. Membr. Sci.*, **528**, 147 (2017).
2. F. Kong, H. Yang, Y. Wu, X. Wang and Y. F. Xie, *J. Membr. Sci.*, **476**, 410 (2015).
3. D. L. Shaffer, J. R. Werber, H. Jaramillo, Sh. Lin and M. Elimelech, *Desalination*, **356**, 271 (2015).
4. A. Zirehpour, A. Rahimpour and M. Ulbricht, *J. Membr. Sci.*, **531**, 59 (2017).
5. Y. Cui, X. Y. Liu, T. Sh. Chung, M. Weber, C. Staudt and Ch. Maletzko, *Water Res.*, **91**, 104 (2016).
6. X. Liu, S. L. Ong and H. Y. Ng, *J. Membr. Sci.*, **511**, 40 (2016).
7. F. Esfandian, M. Peyravi, A. A. Ghoreyshi, M. Jahanshahi and A. Sh. Rad, *Arab. J. Chem* (2017).
8. M. Peyravi, M. Jahanshahi, A. Rahimpour, A. Javadi and S. Hajavi, *Chem. Eng. J.*, **241**, 155 (2014).
9. M. Khajouei, M. Peyravi and M. Jahanshahi, *J. Membr. Sci. Res.*, **3**, 2 (2017).
10. M. Peyravi, A. Rahimpour and M. Jahanshahi, *J. Membr. Sci.*, **423**, 225 (2012).
11. S. Morales-Torres, C. M. Esteves, J. L. Figueiredo and A. M. Silva, *J. Membr. Sci.*, **520**, 326 (2016).
12. D. Li, Y. Yan and H. Wang, *Prog. Poly. Sci.*, **61**, 104 (2016).
13. Sh. Lin, *J. Membr. Sci.*, **514**, 176 (2016).
14. Z. Dabaghian and A. Rahimpour, *Chem. Eng. Res. Design*, **104**, 647 (2015).
15. A. H. Hawari, N. Kamal and A. Altaee, *Desalination*, **398**, 98 (2016).
16. X. Liu and H. Y. Ng, *J. Membr. Sci.*, **469**, 112 (2014).
17. M. Park, J. J. Lee, S. Lee and J. H. Kim, *J. Membr. Sci.*, **375**, 241 (2011).
18. Sh. Chou, R. Wang, L. Shi, Q. She, Ch. Tang and A. G. Fane, *J. Membr. Sci.*, **389**, 25 (2012).
19. Q. Liu, J. Li, Zh. Zhou, J. Xie and J. Y. Lee, *Scientific Reports*, **6**, 1 (2016).
20. Zh. Liu, H. Yu, G. Kang, X. Jie, Y. Jin and Y. Cao, *J. Membr. Sci.*, **497**, 485 (2016).
21. P. Xiao, L. D. Nghiem, Y. Yin, X. Li, M. Zhang, G. Chen, J. Song and T. He, *J. Membr. Sci.*, **481**, 106 (2015).
22. Q. She, X. Jin and Ch. Y. Tang, *J. Membr. Sci.*, **401**, 262 (2012).
23. Ch. Boo, S. Lee, M. Elimelech, Zh. Meng and S. Hong, *J. Membr. Sci.*, **390**, 277 (2012).
24. Ch. Suh and S. Lee, *J. Membr. Sci.*, **427**, 365 (2013).
25. M. F. Jimenez-Solomon, P. Gorgojo, M. Munoz-Ibanez and A. G. Livingston, *J. Membr. Sci.*, **448**, 102 (2013).
26. N. Ma, J. Wei, S. Qi, Y. Zhao, Y. Gao and Ch. Y. Tang, *J. Membr. Sci.*, **441**, 54 (2013).
27. J. Yin and B. Deng, *J. Membr. Sci.*, **479**, 256 (2015).
28. M. Ghanbari, D. Emadzadeh, W. J. Lau, H. Riazi, D. Almasi and A. F. Ismail, *Desalination*, **377**, 152 (2016).
29. M. Tian, Y. N. Wang, R. Wang and A. G. Fane, *Desalination*, **401**, 142 (2017).
30. X. Feng, H. Guo, K. Patel, H. Zhou and X. Lou, *Chem. Eng. J.*, **244**, 327 (2014).
31. M. Abbasian, N. K. Aali and S. E. Shoja, *J. Macromol. Sci.*, **50**, 966 (2013).
32. P. Liu and T. Wang, *Cur. Ap. Phy.*, **8**, 66 (2008).
33. R. R. Darabi, M. Peyravi and M. Jahanshahi and A. A. Q. Amiri, *Korean J. Chem. Eng.*, **34**, 2311 (2017).
34. M. I. Baig, P. G. Ingole, W. K. Choi, J. d. Jeon, B. Jang, J. H. Moon and H. K. Lee, *Chem. Eng. J.*, **308**, 27 (2017).
35. M. Amini, M. Jahanshahi and A. Rahimpour, *J. Membr. Sci.*, **435**, 233 (2013).
36. N. Shafaei, M. Peyravi and M. Jahanshahi, *Polym. Adv. Technol.*, **27**, 1325 (2016).
37. Sh. Ma, L. Shi, X. Feng, W. Yu and B. Lu, *J. Shan. Uni.*, **12**, 278 (2008).
38. A. Anžlovar, Z. C. Orel and M. Žigon, *Eur. Polym. J.*, **46**, 1216 (2010).
39. S. M. Khaled, R. Sui, P. A. Charpentier and A. S. Rizkalla, *Langmuir*,

23, 3988 (2007).
40. J. R. McCutcheon and M. Elimelech, *J. Membr. Sci.*, **318**, 458 (2008).
41. A. Saffar, P. J. Carreau, A. Ajji and M. R. Kamal, *J. Membr. Sci.*, **462**, 50 (2014).
42. M. Peyravi, A. Rahimpour, M. Jahanshahi, A. Javadi and A. Shockravi, *Micropor. Mesopor. Mater.*, **160**, 114 (2012).
43. E. L. Tian, H. Zhou, Y. W. Ren, X. Z. Wang and Sh. W. Xiong, *Desalination*, **347**, 207 (2014).
44. M. Peyravi, A. Rahimpour and M. Jahanshahi, *J. Membr. Sci.*, **473**, 72 (2015).
45. D. Emadzadeh, W. J. Lau and A. F. Ismail, *Desalination*, **330**, 90 (2013).
46. N. Misdan, W. J. Lau, A. F. Ismail and T. Matsuura, *Desalination*, **329**, 9 (2013).
47. Sh. Zhu, S. Zhao, Zh. Wang, X. Tian, M. Shi, J. Wang and Sh. Wang, *J. Membr. Sci.*, **493**, 263 (2015).
48. Sh. Xia, L. Yao, Y. Zhao, N. Li and Y. Zheng, *Chem. Eng. J.*, **280**, 720 (2015).
49. H. Hoseinpour, M. Jahanshahi, M. Peyravi and A. Nozad, *J. Ind. Eng. Chem.*, **46**, 244 (2017).
50. J. Wei, Ch. Qiu, Ch. Y. Tang, R. Wang and A. G. Fane, *J. Membr. Sci.*, **372**, 292 (2011).
51. D. Emadzadeh, W. J. Lau, M. Rahbari-Sisakht, H. Ilbeygi, D. Rana, T. Matsuura and A. F. Ismail, *Chem. Eng. J.*, **281**, 243 (2015).
52. D. Emadzadeh, W. J. Lau, T. Matsuura, A. F. Ismail and M. Rahbari-Sisakht, *J. Membr. Sci.*, **449**, 74 (2014).
53. X. Liu and H. Y. Ng, *J. Membr. Sci.*, **469**, 112 (2014).
54. O. Akin and F. Temelli, *Desalination*, **278**, 387 (2011).
55. W. Kuang, Zh. Liu, G. Kang, D. Liu, M. Zhou and Y. Cao, *J. Appl. Poly. Sci.*, **133**, 1 (2016).

Supporting Information

Sublayer assisted by hydrophilic and hydrophobic ZnO nanoparticles toward engineered osmosis process

Sina Mansouri*, Soodabeh Khalili, Majid Peyravi**, Mohsen Jahanshahi**,†, Rezvaneh Ramezani Darabi**, Fatemeh Ardeshiri***, and Ali Shokuhi Rad*****

*School of Chemical Engineering, Kavosh Institute of Higher Education, Mahmood Abad, Iran
**Membrane Research Group, Nanotechnology Institute, Babol Noshirvani University of Technology, Shariati Ave., Babol, 47148-71167, Iran
***Institute of Nanoscience and Nanotechnology, University of Kashan, Kashan, Iran
****Department of Chemical Engineering, Qaemshahr Branch, Islamic Azad University, Qaemshahr, Iran
(*Received 31 December 2017 • accepted 27 May 2018*)

Preparation of Sublayer

Table 1 demonstrates the characteristics of nine sublayers prepared in the current study using PES-based casting solutions [1]. All membrane sublayers were successfully prepared using a phase inversion method. For the preparation of pure PES solution, PVP was first added into DMF and stirred for 15 min. A stipulated amount of dried PES was dissolved in DMF for at least 12 hr until the casting solution became homogeneous. The prepared mixture was then degassed at 25 °C for 5 hr until air bubbles trapped in the dope solution could be removed. The clear casting solution was spread on a clean glass plate and cast by stainless steel casting knife. Afterwards, the casting film was quickly and smoothly immersed into the DI water coagulation bath at 30 °C where phase inversion took place. Then PES membrane got separated from the clean glass plate, it was submerged into another DI water coagulation bath for 1 day to remove residual DMF solvent and stored in DI water before use. For the preparation of hydrophilic and hydrophobic sublayers, ZnO nanoparticles alongside PVP were dispersed in DMF via sonication for 30 min before adding PES into the homogeneous casting solution. The next preparation steps are as same as the procedure presented above for pure PES sublayer.

Preparation of Rejection Layer

The polyamide rejection layer was formed by interfacial polymerization (IP) on top of the hand-cast PES sublayer according to our previous work [1]. In brief, the polyamide TFC and TFN membranes was fabricated by first immersing the PES sublayer in a 2.0 wt% MPD- DI water solution for 2 min. The remaining MPD solution was carefully and slowly removed from the sublayer surface by a rubber roller. Next, the MPD saturated sublayer was immersed in a 0.1 wt% of TMC-nhexane solution for 30 s to form the ultrathin active layer. Then, the TFC and TFN membranes weredried in an oven at 80 °C for 5 min and stored in DI water container before FO/RO measurements.

Dispersion of the Hydrophilic and Hydrophobic Nanoparticles

The hydrophilicity and hydrophobicity of the ZnO nanoparticles was studied by the dispersibility of hydrophilic and hydrophobic ZnO nanoparticles in both water and n-hexane solvent [2]. For the preparation suspensions, 0.01 gr of hydrophilic and hydrophobic ZnO nanoparticles was added in two solvent (10 ml) and sonicated for 15 min at 25 °C. Afterward, suspensions were stood at ambient temperature for 20 hr.

Evaluation of Membrane Performance

RO experimental setup in a cross-flow filtration mode was used to determine pure water permeability and selectivity of the TFC and TFN membranes. The permeation plexiglass cell was designed to have an effective filtration area of 39.5 cm^2. RO experimental filtration tests were carried out using FS containing 20 mM NaCl in water at 2.5 bar. Pure water flux (J, L/m^2 h) and pure water permeability (A, L/m^2 h bar) [3] of the TFC and TFN membranes were calculated according to following Eqs.:

$$J = \frac{\Delta V}{A_m \cdot \Delta t}$$

$$A = \frac{J}{\Delta P}$$

Where A_m is an effective area of FO membrane, ΔV is the volume of permeate, Δt is RO process time and ΔP is applied pressure difference. To evaluate membrane salt rejection, Eq. (3) was employed as fallows [4]:

$$R = \left(1 - \frac{C_p}{C_f}\right) \times 100$$

Where C_f (mol/L) is the concentration of NaCl salt in the FS and C_p (mol/L) indicates the permeate solution. The term salt permeability (B, L/m^2 h) [5] was used to study the FO membrane behavior in terms of NaCl salt rejection. B is calculated during RO experiment by the following equation:

$$\frac{1-R}{R} = \frac{B}{A(\Delta P - \Delta \pi)}$$

Where $\Delta\pi$ is the osmotic pressure gradient across the semi-permeable membrane.

The FO pure water flux and salt flux as the most common performance examinations for TFC and TFN membranes were mea-

sured via a laboratory-scale FO setup. The laboratory setup contained a FO membrane test plexiglass cell with an effective membrane area of 39 cm^2. Two diaphragm pumps circulated FS and DS on both sides of the plexiglass cell. Both FS and DS were circulated at a same cross flow rate of 800 ml/min. Aqueous 10 mM and 2 M NaCl salt solution were used as the FS and DS, respectively. A digital weight balance was located at the bottom of the FS tank to precisely measure the pure water flux of the FO membrane. With respect to NaCl rejection rate, a conductivity meter (WA-2017SD, Taiwan) was applied to measure the conductivity of DS and was later converted into NaCl concentration in accordance to conductivity vs NaCl concentration calibration curve. All measurements were performed at ambient temperature for three times and the average data were reported. The FO pure water flux (J_v, L/m^2·h) was calculated by measuring the weight change of FS [6]:

$$J_v = \frac{\Delta V}{A_m \cdot \Delta t} = \frac{\Delta m/\rho}{A_m \cdot \Delta t}$$

In this equation, ΔV (L) is the volume change of FS, A_m (m^2) is membrane surface area, Δt (h) is the time interval, Δm is the weight change of FS and ρ is the density of FS. After the FO experimental setup reached stability in 30 min, the change in NaCl salt concentration of FS was used to calculate the reverse salt flux (J_s, g/m^2h) by the following equation [7]:

$$J_s = \frac{V_t C_t - V_0 C_0}{A_m \cdot \Delta t}$$

Where C_0 and V_0 are the initial NaCl salt concentration and volume of the FS, respectively. C_t and V_t are the NaCl concentration and the volume of the FS at the end of FO experimental test, respectively. The membrane *S* parameter is an intrinsic FO membrane property used to demonstrate the extent of ICP which influences the FO membranes performance. In the FO processes, the *S* parameter is determined using following equations:

$$J_v = \frac{D}{S}\left[\mathrm{Ln}\frac{A\pi_{draw} + B}{A\pi_{feed} + B + J_v}\right]$$

Where D (m^2/s) is the diffusivity of the DS, π_{draw} and π_{feed} indicate the osmotic pressures of the DS and FS, respectively [6].

REFERENCES

1. R. R. Darabi, M. Peyravi, M. Jahanshahi and A. A. Q. Amiri, *Korean J. Chem. Eng.*, **34**, 2311 (2017).
2. Y. Ahmad Nor, Y. Niu, S. Karmakar, L. Zhou, C. Xu, J. Zhang, H. Zhang, M. Yu, D. Mahony, N. Mitter, M. A. Cooper and Ch. Yu, *ACS Cent. Sci.*, **1**, 328 (2015).
3. Z. Dabaghian, A. Rahimpour and M. Jahanshahi, *Desalination*, **381**, 117 (2016).
4. H. Hoseinpour, M. Peyravi, A. Nozad and M. Jahanshahi, *J. Taiwan Inst. Chem. Engineers*, **67**, 453 (2016).
5. A. Zirehpour, A. Rahimpour, F. Seyedpour and M. Jahanshahi, *Desalination*, **371**, 46 (2015).
6. N. Niksefat, M. Jahanshahi and A. Rahimpour, *Desalination*, **343**, 140 (2014).
7. X. Liu and H. Y. Ng, *J. Membr. Sci.*, **481**, 148 (2015).